Available online at www.sciencedirect.com

SciVerse ScienceDirect

Ceramics International 39 (2013) 6319–6324

CERAMICS INTERNATIONAL

www.elsevier.com/locate/ceramint

# White light emission from $Eu^{3+}$ co-activated $Ca_2Gd_8Si_6O_{26}$:$Dy^{3+}$ nanophosphors by solvothermal synthesis

E. Pavitra, G. Seeta Rama Raju, Jae Su Yu*

*Department of Electronics and Radio Engineering, Institute for Laser Engineering, Kyung Hee University, 1 Seocheon-dong, Giheung-gu, Yongin-si, Gyeonggi-do 446-701, Republic of Korea*

Received 30 December 2012; received in revised form 4 January 2013; accepted 17 January 2013
Available online 1 February 2013

**Abstract**

$Ca_2Gd_8(SiO_4)_6O_2$ (CGS) nanophosphors with different concentrations of single-doped $Dy^{3+}$ ions and co-doped $Dy^{3+}/Eu^{3+}$ ions were prepared by a solvothermal synthesis. Very fine particles in the nanometer range could be achieved by this method, as evidenced by transmission electron microscope measurements. The hexagonal phase of the oxyapatite structure was confirmed by X-ray diffraction patterns. The energy transfer between $Eu^{3+}$ and $Dy^{3+}$ ions was investigated by photoluminescence excitation and emission properties. These phosphors had absorption bands in the UV and NUV region, which are suitable for the emission wavelength of UV or NUV light-emitting diodes (LEDs). With increasing the $Eu^{3+}$ ion concentration, the emission peak intensity corresponding to the $^5D_0 \rightarrow {}^7F_2$ transition increased and the yellow ($^4F_{9/2} \rightarrow {}^6H_{13/2}$) emission intensity also increased compared to the blue ($^4F_{9/2} \rightarrow {}^6H_{15/2}$) emission intensity due to the increased energy transfer between $Dy^{3+}$ to $Eu^{3+}$ ions. Thus, the $Eu^{3+}$ ions compensated the red emission component of the $Dy^{3+}$ doped CGS nanophosphors. Such phosphors are expected to have potential applications for NUV based white LEDs.



*Keywords:* C. Optical properties; D. Apatite; Solvothermal process; White light emission

## 1. Introduction

Solid-state lighting becomes a smart strategy for energy saving, safety (lack of toxic mercury), reliability, maintenance, and eco-friendly characteristics, with its promise of being about 10 times more efficient than the incandescent lighting [1–3]. Besides, oxide-based phosphors activated with trivalent rare-earth ions are particularly important in the application of generating artificial light for next-generation field-emission display devices and white light-emitting diodes (WLEDs) due to their stable physical and chemical properties. At present, primarily two general approaches are being explored to yield WLEDs: blue LED chip coated with yellow phosphor and the tri-band (red, green, and blue) based WLEDs, which have been fabricated by pumping with UV-A (320–400 nm) LED sources [4–6]. In both approaches, highly-efficient and long-lived phosphor materials that are well matched to the excitation conditions of the diode should be necessarily developed and thus their spectral emission properties produce a high color rendering index ( > 95).

Recently, among the various kinds of synthetic oxyapatites, the ternary rare-earth-metal silicate with the oxyapatite structure of $Ca_2$ $RE_8$ $(SiO_4)_6O_2$ (RE = Y/Gd) as an efficient host lattice for well-organized excitation induced tunable luminescent properties of various rare-earth (RE) ions and mercury-like ions [7]. The ternary CGS host lattice belongs to the family of oxyapatite $M^I_4$ $M^{II}_6$ $(XO_4)_6O_2$ hexagonal structures with space group $P6_3/m$, where $M^I$ and $M^{II}$ positions correspond to the two distinct low symmetry ($C_3$ and $C_s$) crystallographic sites, which accommodate metal ions such as divalent alkaline-earth or $RE^{3+}$ elements. In the CGS host lattice, $Ca^{2+}$ and $Gd^{3+}$ ions are randomly distributed in the $C_3$ point symmetry of the 9-fold coordinated 4f site, and $Gd^{3+}$ ions are completely occupied in the $C_s$ point symmetry of 7-fold coordinated 6h sites. Both sites are very suitable for the luminescence of $RE^{3+}$ ions owing

*Corresponding author. Tel.: +82 31 201 3820; fax: +82 31 206 2820.
*E-mail address:* jsyu@khu.ac.kr (J.S. Yu).

0272-8842/$ - see front matter © 2013 Elsevier Ltd and Techna Group S.r.l. All rights reserved.
http://dx.doi.org/10.1016/j.ceramint.2013.01.057

to their low symmetry features. The X-site is occupied by P-block elements such as P, As, Si, or Ge [2,8].

Among the $RE^{3+}$ ions, dysprosium ($Dy^{3+}$) ions exhibit strong luminescence in a variety of lattices, leading to both blue ($^4F_{9/2} \rightarrow {}^6H_{15/2}$) and yellow ($^4F_{9/2} \rightarrow {}^6H_{13/2}$) emissions. By appropriate adjustment of yellow-to-blue intensity ratio ($Y/B$) values, it is possible to obtain near-white emission [9,10]. But, unfortunately, $Dy^{3+}$ single-doped CGS phosphors suffer from a lack of red component. In order to compensate the red component, $Eu^{3+}$ ions were also introduced into CGS host lattice because it is one of the most important activators among RE ions due to the rich red emission from the $^5D_0 \rightarrow {}^7F_2$ transition [10].

To the best of our knowledge, until now, no reports have been found on the detailed luminescent properties of $Dy^{3+}$ single-doped and $Eu^{3+}/Dy^{3+}$ co-doped CGS nanophosphors by a solvothermal process. It is well known that the phosphors with fine particle size and narrow size distribution offer the possibility of high resolution and high luminescence efficiency. In this work, the structural and detailed luminescence properties of $Dy^{3+}$ single-doped and $Dy^{3+}/Eu^{3+}$ co-doped nanophosphor samples by varying the concentrations were systematically investigated and the energy transfer between the $Dy^{3+}$ and $Eu^{3+}$ ions was also discussed.

## 2. Experimental details

Nanocrystalline CGS host lattices doped with $Dy^{3+}$ and $Eu^{3+}$ ions were prepared by the solvothermal process with the composition of $Ca_2(Gd_{8-(x+y)}\ Dy_x\ Eu_y)Si_6O_{26}$ ($x=0.5$, 1, 2 mol%; $y=1$, 2, 3 mol%). The appropriate amounts of high-purity grade calcium nitrate tetrahydrate ($Ca(NO_3)_2 \cdot 4H_2O$), gadolinium nitrate hexahydrate ($Gd(NO_3)_3 \cdot 6H_2O$), dysprosium nitrate pentahydrate ($Dy(NO_3)_3 \cdot 5H_2O$), europium nitrate pentahydrate ($Eu(NO_3)_3 \cdot 5H_2O$), and tetraethyl orthosilicate ($Si(OC_2H_5)_4$) were dissolved in 70 ml of 2-propanol. All reagents were taken without any further purification and stirred vigorously using the magnetic stirrer until the formation of homogeneous solution and then transferred into a stainless steel autoclave with a Teflon liner (140 ml capacity and 50% filling). Then, it was heated to 230 °C at a rate of 2 °C/min and maintained for 5 h with continued magnetic stirring (at 180 rpm) to make stable networks between the reactants. After gradually cooling down to room temperature, the precipitate was separated by a centrifugal separator with 5000 rpm for 5 min and then dried at 100 °C for a day in ambient atmosphere. Finally, the dried powder was annealed at 1200 °C for 5 h. The experiment was repeated at similar conditions as functions of $Dy^{3+}$ and $Eu^{3+}$ ion concentrations.

The X-ray diffraction (XRD) patterns of the CGS samples were recorded by using a powder X-ray diffractometer (Mac Science, M18XHF-SRA) with Cu$K$=1.5406 Å. The morphology of the samples was examined by using a field-emission transmission electron microscope (FE-TEM: JEOL, JEM-2100F). The Fourier transform infrared (FTIR) spectra of the CGS samples were measured by using a Thermo Nicolet-5700 spectrophotometer. The room-temperature photoluminescence (PL) spectra were recorded on a Photon Technology International (PTI, USA) fluorimeter with a Xe-arc lamp of power 60 W.

## 3. Results and discussion

Fig. 1 shows the XRD patterns of pure CGS, CGS:$Dy^{3+}$ and CGS:$Dy^{3+}/Eu^{3+}$ nanophosphors sintered at 1200 °C. All the diffraction peaks correspond to the hexagonal phase of the oxyapatite structure with space group $P6_3/m$, which are in well agreement with the standard JCPDS card [PDF (28-0212)]. No impurity phase caused by RE ions can be noticed at the current doping level, indicating that the $Dy^{3+}$ and $Eu^{3+}$ ions are completely dissolved into the $Gd^{3+}$ sites of CGS host lattice. It is well known that the pure phase is favorable for luminescent properties of phosphors. Generally, the crystallite size can be estimated by using the Scherrer equation, $D_{hkl}=(k\lambda)/(\beta \cos \theta)$, where $D$ is the average grain size, $k$(0.9) is a shape factor, $\lambda$ is the X-ray wavelength (1.5406 Å), and $\beta$ and $\theta$ are the full width at half maximum and the diffraction angle of an observed peak, respectively. The strongest diffraction peaks were used to calculate the crystallite sizes of CGS nanophosphors sintered at 1200 °C, which yields an average value of about 72 nm. The crystallainity of the CGS phosphors with different concentrations of $Eu^{3+}/Dy^{3+}$ ions was the same because the energy supply was constant. The inset of Fig. 1 shows the TEM image of the CGS:1 mol% $Dy^{3+}$ (i.e., CGS:1$Dy^{3+}$) sample annealed at 1200 °C. From the TEM image, it is clear that the particles are in the nanometer range.

The FTIR spectrum of the CGS:1$Dy^{3+}$ nanophosphors annealed at 1200 °C is shown in Fig. 2. Typically, the bands at 3572 $cm^{-1}$ and 630 $cm^{-1}$ originated from the

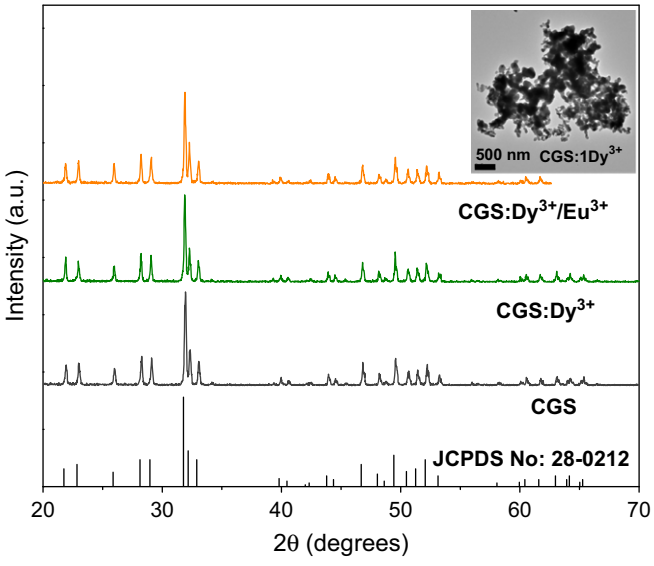


Fig. 1. XRD patterns of pure CGS, $Dy^{3+}$ single-doped CGS, and $Dy^{3+}/Eu^{3+}$ co-doped CGS nanophosphors (inset shows the TEM image of CGS:1$Dy^{3+}$).

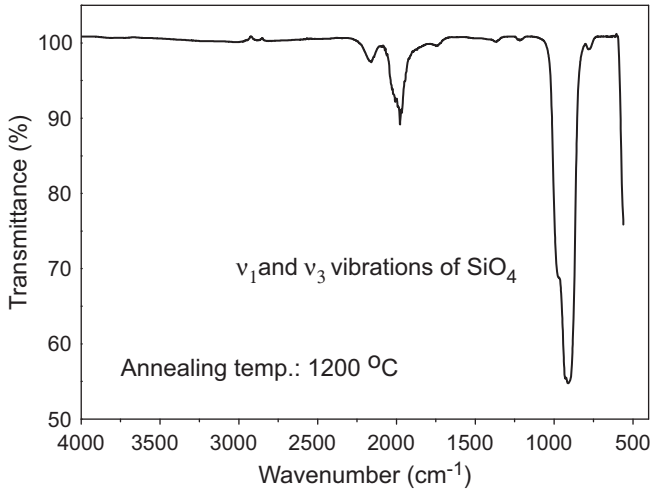


Fig. 2. FTIR spectrum of the CGS:1Dy$^{3+}$ nanophosphors annealed at 1200 °C.

O–H stretching and librational modes, respectively, have been observed in hydroxyapatite structure. However, here no absorption bands were observed at 3572 cm$^{-1}$ and 630 cm$^{-1}$, suggesting that the successful formation of the oxyapatite phase in our samples. For $SiO_4$ units, the IR absorption bands can be assigned based on four kinds of modes: symmetric ($v_1$) and anti-symmetric ($v_3$) stretching modes, and symmetric ($v_2$) and anti-symmetric ($v_4$) bending modes. The stretching vibrations, $v_1$ and $v_3$, which were overlapped with each other and gives a fairly intense broad absorption band at wavelengths between 2000 and 800 cm$^{-1}$. This result is in agreement with the previously reported IR absorption data of the $SiO_4$ units in the apatite structure [11,12].

Fig. 3(a) shows the PL excitation (PLE) spectra of CGS:Dy$^{3+}$ nanophosphors as a function of Dy$^{3+}$ ion concentration by monitoring the emission wavelength at 574 nm. The spectrum consists of strong excitation band at 275 nm and somewhat weak band at 307 nm occurred due to the f–f transitions of Gd$^{3+}$ ions corresponding to the electronic transitions of $^8S_{7/2}\rightarrow{}^6I_{11/2}$ and $^8S_{7/2}\rightarrow{}^6I_{7/2}$, respectively. This means that highly-efficient energy transfer occurred between Gd$^{3+}$ and Dy$^{3+}$ ions. The spectrum also consisted of some sharp bands in the longer wavelength region due to the f–f transitions of Dy$^{3+}$ ions within its 4f$^9$ configuration, which are assigned to the electronic transitions: ($^6H_{15/2}\rightarrow(^4D^4G)_{5/2}$) at 313 nm, ($^6H_{15/2}\rightarrow{}^6P_{3/2}$) at 323 nm, ($^6H_{15/2}\rightarrow{}^6P_{7/2}$) at 350 nm, ($^6H_{15/2}\rightarrow{}^6P_{5/2}$) at 363 nm, ($^6H_{15/2}\rightarrow{}^4I_{13/2}$) at 387 nm, ($^6H_{15/2}\rightarrow{}^4G_{11/2}$) at 426 nm, and ($^6H_{15/2}\rightarrow{}^4I_{15/2}$) at 451 nm. From the PLE spectra, it is clear that by increasing the Dy$^{3+}$ ion concentration from 0.5 to 3 mol%, the intensity of peaks originated from the Gd$^{3+}$ ions decreased whereas the intensity of peaks originated from the Dy$^{3+}$ ions increased due to the change of Dy$^{3+}$ polarization of the surrounding $O^{2-}$ ions in the host lattice [9,13].

Fig. 3(b) shows the PL emission spectra of CGS:Dy$^{3+}$ nanophosphors with different concentrations of Dy$^{3+}$ ions by monitoring the excitation wavelength at 275 nm. The

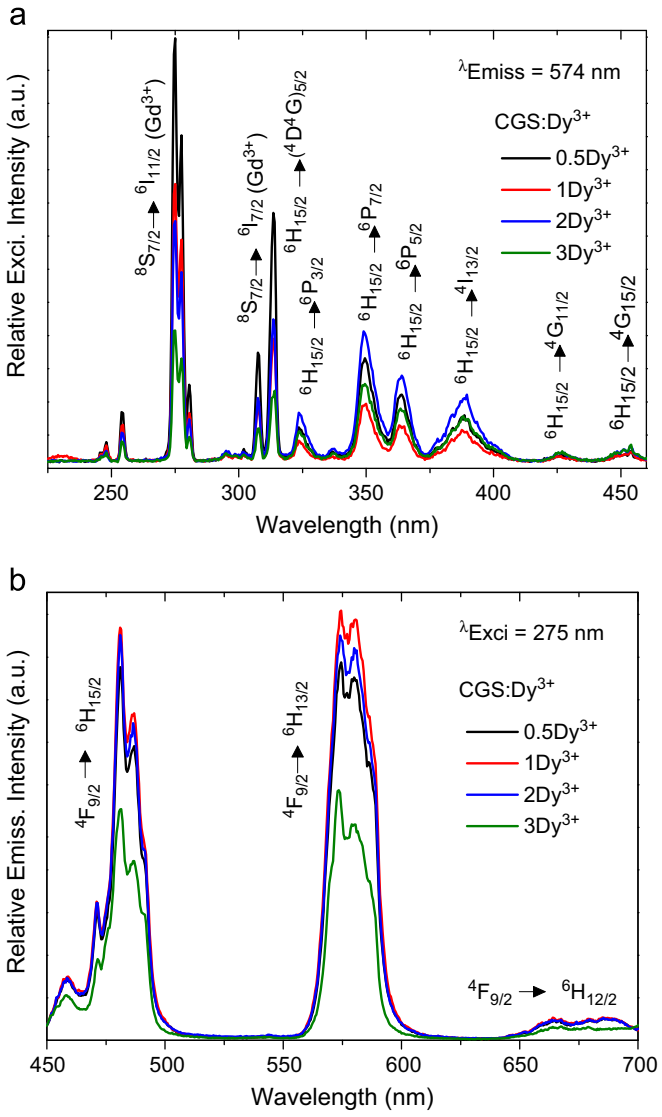


Fig. 3. (a) PLE and (b) PL emission spectra of CGS:Dy$^{3+}$ nanophosphors with different Dy$^{3+}$ ion concentrations. (For interpretation of the references to color in this figure legend, the reader is referred to the web version of this article.)

emission spectra exhibited two main groups of bands in the blue (460–500 nm) and yellow (555–610 nm) regions. Some weak bands were also observed in the red region. These blue, yellow, and red emissions are assigned to the electronic transitions of $^4F_{9/2}\rightarrow{}^6H_{15/2}$, $^4F_{9/2}\rightarrow{}^6H_{13/2}$, and $^4F_{9/2}\rightarrow{}^6H_{11/2}$, respectively. The blue ($^4F_{9/2}\rightarrow{}^6H_{15/2}$) emission corresponds to the magnetic dipole transition and the yellow ($^4F_{9/2}\rightarrow{}^6H_{13/2}$) emission is related to the hypersensitive (forced electric dipole) transition. The crystal field splitting components of Dy$^{3+}$ ions can be observed, which indicates that Dy$^{3+}$ ions are well substituted into Gd$^{3+}$ sites because the ionic radius of the Dy$^{3+}$ (1.03 Å) ions is smaller than that of the Gd$^{3+}$ (1.05 Å) ions. In this CGS:Dy$^{3+}$ nanophosphor, the integrated intensity of yellow emission is greater than that of the blue emission. This can be explained by the well-known fact that the hypersensitive (forced electric dipole) transition is strongly influenced by the outside surrounding

environment and the magnetic dipole transition is insensitive to the crystal field strength around the $Dy^{3+}$ ions. When $Dy^{3+}$ is located at a low symmetry local site (without inversion symmetry), the yellow emission is often dominant in the emission spectrum. When $Dy^{3+}$ is at a high symmetry local site (with inversion symmetry center), the blue emission is stronger than the yellow emission and is dominant in the emission spectrum. When the concentration of $Dy^{3+}$ ions increased to 1 mol%, the emission reached its maximum intensity. Above 1 mol%, with increasing the $Dy^{3+}$ ion concentration, the emission intensities decreased remarkably due to the concentration quenching. This is caused by the migration of excitation energy between the emission ions or the loss of excitation energy by non-radiative transition.

The PLE and PL spectra of $Eu^{3+}$ single-doped CGS nanophosphors with different ion concentrations were previously reported [11]. The PLE spectra of the $1Dy^{3+}/3Eu^{3+}$ co-doped CGS nanophosphors by monitoring with both the emission wavelengths at 615 and 578 nm corresponding to the $^5D_0 \rightarrow {}^7F_2$ and $^4F_{9/2} \rightarrow {}^4H_{13/2}$ transitions of $Eu^{3+}$ and $Dy^{3+}$, respectively, are shown in Fig. 4(a). These two PLE spectra were measured under the same experimental conditions. The both spectra consisted of a broad excitation band in the shorter wavelength region due to the charge transfer between the completely filled 2p orbital of $O^{2-}$ ions and partially filled 4f orbital of the $Eu^{3+}$ ions (i.e., CBT), and some sharp excitation bands in the longer wavelength region due to the f–f transitions of $Eu^{3+}$ ions assigned to the electronic transitions of $^7F_0 \rightarrow {}^5D_4$ at 363 nm, $^7F_0 \rightarrow {}^5G_3$ at $_3$76 nm, $^7F_0 \rightarrow {}^5G_4$ at 383 nm, $^7F_0 \rightarrow {}^5L_6$ at 395 nm, $^7F_0 \rightarrow {}^5D_3$ at 414 nm, and $^7F_0 \rightarrow {}^5D_2$ at 464 nm. Due to the f–f transitions of $Dy^{3+}$ ions, the electronic transitions of $^6H_{15/2} \rightarrow {}^5P_{7/2}$ at 350 nm, $^6H_{15/2} \rightarrow {}^5P_{5/2}$ at 367 nm, $^6H_{15/2} \rightarrow {}^4G_{11/2}$ at 427 nm, and $^6H_{15/2} \rightarrow {}^4I_{15/2}$ at 454 nm were observed [13,14]. It is noticeable that the both $Eu^{3+}$ and $Dy^{3+}$ excitation bands were observed when exciting with red and yellow radiations. The reason is that the tail of $^4F_{9/2} \rightarrow {}^4H_{13/2}$ emission of $Dy^{3+}$ ions almost overlapped with the $^5D_0 \rightarrow {}^7F_0$ emission of $Eu^{3+}$ ions and virtually suppressed emission of $Dy^{3+}$ ions overlapped with strong $^5D_0 \rightarrow {}^7F_2$ emission of $Eu^{3+}$ ions. This situation also clarified that the peaks exhibited higher intensities by monitoring with the yellow emission wavelength of 578 nm than by monitoring with the red emission wavelength of 615 nm. These spectral features worthily mean that an efficient energy transfer between the $Dy^{3+}$ and $Eu^{3+}$ ions in the co-doped sample is possible.

Fig. 4(b) shows the PL emission spectra of $Dy^{3+}/Eu^{3+}$ co-doped CGS nanophosphors as a function of $Eu^{3+}$ ion concentration by exciting at 383 nm whereas the $Dy^{3+}$ ion concentration is fixed at 1 mol%. Here, we used 383 nm as excitation wavelength instead of 274 nm because, if the excitation source of 274 nm is used, the red emission is dominant rather than the $Dy^{3+}$ emission due to the strong interaction between $Eu^{3+}$ and $O^{2-}$ ions. In the case of 383 nm, however, the $Dy^{3+}$ and $Eu^{3+}$ excitation efficiencies were almost equal and useful for color rendering property.

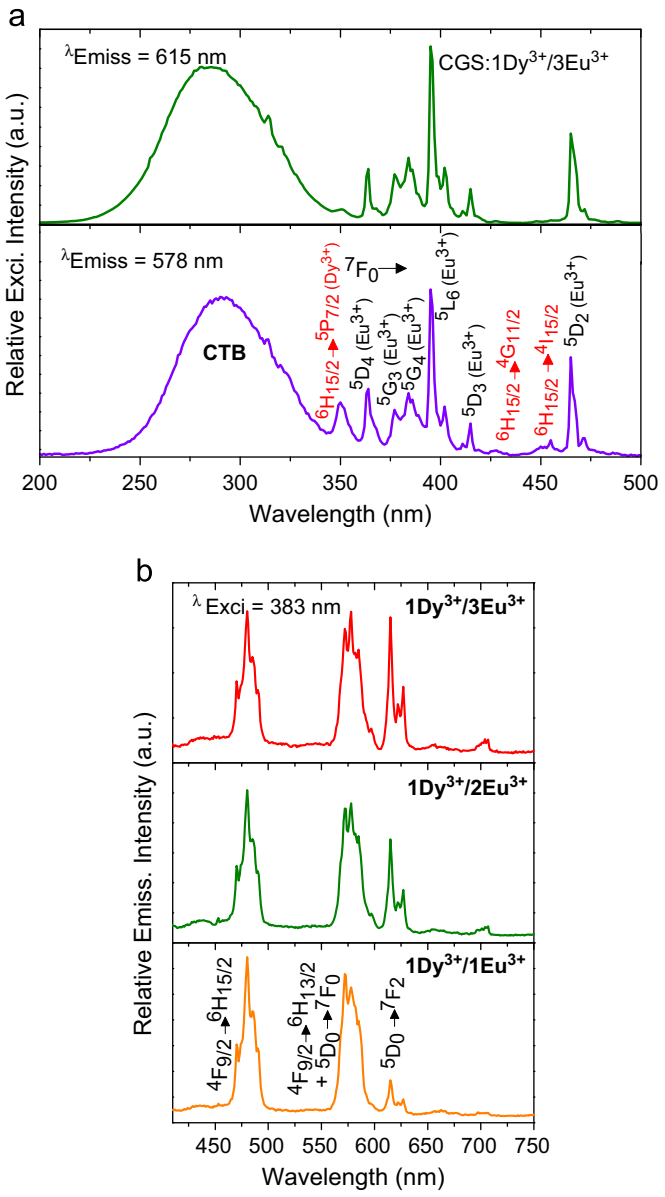


Fig. 4. (a) PLE spectra of $1Dy^{3+}/3Eu^{3+}$ co-doped CGS nanophosphors by monitoring the emission wavelengths at 578 (yellow) and 615 nm (red) and (b) PL emission spectra of $Dy^{3+}/Eu^{3+}$ co-doped CGS nanophosphors at different $Eu^{3+}$ ion concentrations. (For interpretation of the references to color in this figure legend, the reader is referred to the web version of this article.)

Moreover, for efficient phosphor converted WLEDs, this excitation wavelength can be easily obtained by near UV/blue excitation sources such as InGaN-based LED chips [15]. From the PL emission spectra, three intense emission peaks corresponding to the $^4F_{9/2} \rightarrow {}^6H_{15/2}$ transition at 479 nm, $^4F_{9/2} \rightarrow {}^6H_{13/2}$ transition at 572 nm, and $^5D_0 \rightarrow {}^7F_2$ transition at 615 nm were observed and a week emission peak by the $^5D_0 \rightarrow {}^7F_1$ transition also appeared. By increasing the $Eu^{3+}$ ion concentration, the emission peak intensity corresponding to the $^5D_0 \rightarrow {}^7F_2$ transition increased due to the increased energy transfer from $Dy^{3+}$ to $Eu^{3+}$ ions. However, simultaneously, the $^4F_{9/2} \rightarrow {}^6H_{13/2}$ transition at 578 nm also increased

compared to 572 nm and the $^4F_{9/2} \rightarrow {}^6H_{15/2}$ transition at 479 nm due to the overlap of the tail of the $Dy^{3+}$ emission peak occurred at 578 nm with the emission band by the $^5D_0 \rightarrow {}^7F_0$ transition of $Eu^{3+}$ ions. This result suggests that a proper concentration of $Eu^{3+}$ ions can compensate the red component in $Dy^{3+}$ doped CGS phosphors. The energy transfer efficiency from $Dy^{3+}$ to $Eu^{3+}$ ions was calculated by the a equation of $\eta = 1 - I_s/I_{so}$ [16,17], where $I_{so}$ and $I_s$ are the integrating emission intensities of the hypersensitive $^4F_{9/2} \rightarrow {}^6H_{13/2}$ transition of $Dy^{3+}$ ions at 578 nm in the absence and presence of $Eu^{3+}$ ions, respectively. The calculated energy transfer efficiencies were 17.22, 35.83, and 57.09 for $1Dy^{3+}/1Eu^{3+}$, $1Dy^{3+}/2Eu^{3+}$, and $1Dy^{3+}/3Eu^{3+}$, respectively. The energy transfer efficiency from $Dy^{3+}$ to $Eu^{3+}$ ions is found to be more prominent at higher $Eu^{3+}$ ion concentration.

The Commission International De I'Eclairage (CIE) chromaticity coordinates of $Dy^{3+}$ single-doped and $Dy^{3+}/Eu^{3+}$ co-doped CGS nanophosphors are presented in Fig. 5. These phosphors exhibited excellent CIE coordinates, which are all in the white emission region. The $Dy^{3+}$ single-doped CGS showed the chromaticity coordinates in the cool white region (0.331, 0.337) and when increasing the $Eu^{3+}$ ion concentration, the chromaticity coordinates were shifted to warm white color region due to the stronger Eu doping effect. The calculated chromaticity coordinates were (0.339, 0.339), (0.356, 0.342), and (0.374, 0.3416) for $1Dy^{3+}/1Eu^{3+}$, $1Dy^{3+}/2Eu^{3+}$, and $1Dy^{3+}/3Eu^{3+}$, respectively. The above results hint the promising application of CGS:$Dy^{3+}/Eu^{3+}$ nanophosphors to make white light for NUV-LEDs as well as optical display systems.

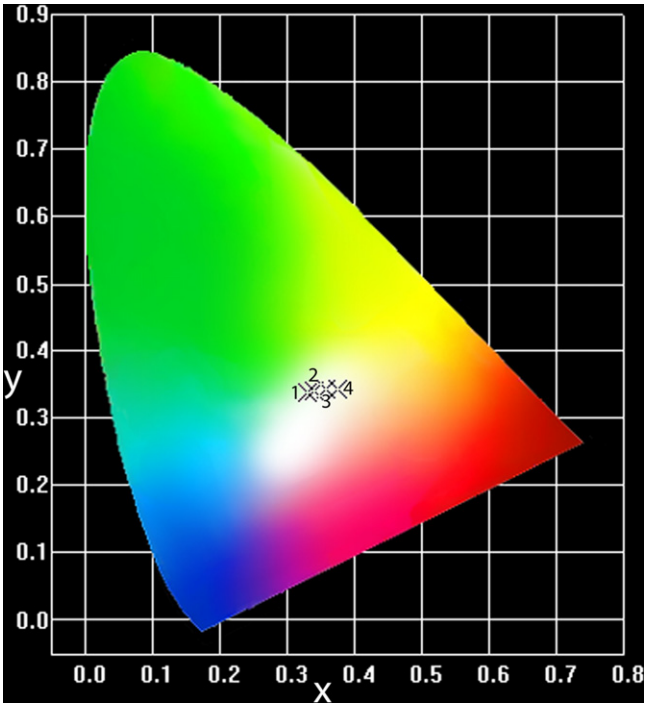


Fig. 5. CIE chromaticity coordinates of $Dy^{3+}$ single-doped and $Dy^{3+}/Eu^{3+}$ co-doped CGS nanophosphors [(1) $1Dy^{3+}$ (2) $1Dy^{3+}/1Eu^{3+}$, (3) $1Dy^{3+}/2Eu^{3+}$, and (4) $1Dy^{3+}/3Eu^{3+}$].

## 4. Conclusions

We have successfully synthesized the $Dy^{3+}$ single-doped and $Dy^{3+}/Eu^{3+}$ co-doped CGS nanophosphors by means of the solvothermal synthesis. The XRD patterns of these phosphors confirmed their hexagonal structure and the TEM measurements showed that the particles were in nano-range order. For $Dy^{3+}$ single-doped CGS nanophosphors, the PL emission spectra showed two strong bands in the blue ($^4F_{9/2} \rightarrow {}^6H_{15/2}$) and yellow ($^4F_{9/2} \rightarrow {}^6H_{15/2}$) regions and the concentration quenching was occurred at 1 mol%. From the luminescence properties of $Dy^{3+}/Eu^{3+}$ co-doped samples, it is found that a white-light emission in a single phase was achieved by monitoring the excitation wavelength at 383 nm which can be excited by UV or NUV LEDs. The energy transfer between the $Eu^{3+}$ and $Dy^{3+}$ ions was observed and by introducing a proper amount of $Eu^{3+}$ ions in CGS:$Dy^{3+}$ phosphors, it may provide a promising way to get natural white light for indoor applications.

## Acknowledgements

This research was supported by Basic Science Research Program through the National Research Foundation of Korea (NRF) funded by the Ministry of Education, Science and Technology (MEST) (No. 2012-0007411).

## References

[1] J. Sun, J. Lai, J. Zhu, Z. Xia, H. Du, Luminescence properties and energy transfer investigations of $Sr_2B_2O_5:Ce^{3+},Tb^{3+}$ phosphors, Ceramics International 38 (7) (2012) 5341–5345.

[2] G. Seeta Rama Raju, J.Y. Park, H.C. Jung, E. Pavitra, B.K. Moon, J.H. Jeong, J.S. Yu, J.H. Kim, H. Choi, Blue and green emissions with high color purity from nanocrystalline $Ca_2Gd_8Si_6O_{26}$:Ln (Ln=Tm or Er) phosphors, Journal of Alloys and Compounds 509 (27) (2011) 7537–7542.

[3] C. Shen, Y. Yang, S. Jin, J. Ming, H. Feng, Z. Xu, White light-emitting diodes using blue and yellow–orange-emitting phosphors, Optik 121 (16) (2010) 1487–1491.

[4] J. Yu, C. Guo, Z. Ren, J. Bai, Photoluminescence of double-color-emitting phosphor $Ca_5(PO_4)_3Cl:Eu^{2+}$, $Mn^{2+}$ for near-UV LED, Optics & Laser Technology 43 (4) (2011) 762–766.

[5] E. Pavitra, J. Su Yu, Luminescent properties of $Gd^{3+}$ sensitized low-phonon energy $CaGd_4O_7:Tb^{3+}$ green emitting novel phosphors, Ceramics International 39 (2) (2013) 1029–1036.

[6] T.-W. Kuo, W.-R. Liu, T.-M. Chen, High color rendering white light-emitting-diode illuminator using the red-emitting $Eu^{2+}$-activated CaZnOS phosphors excited by blue LED, Optics Express 18 (8) (2010) 8187–8192.

[7] X.M. Han, J. Lin, H.L. Zhou, M. Yu, Y.H. Zhou, M.L. Pang, Effects $R^{3+}$ on the photoluminescent properties of $Ca_2$ $R_8$ $(SiO_4)_6$ $O_2$:A (R=Y,La,Gd;A=$Eu^{3+}$,$Tb^{3+}$) phosphor films prepared by the sol–gel process, Journal of Physics: Condensed Matter 16 (15) (2004) 2745.

[8] G.S.R. Raju, Y.H. Ko, E. Pavitra, J.S. Yu, J.Y. Park, H.C. Jung, B.K. Moon, Formation of $Ca_2Gd_8(SiO_4)_6O_2$ nanorod bundles based on crystal splitting by mixed solvothermal and hydrothermal reaction methods, Crystal Growth & Design 12 (2) (2011) 960–969.

[9] G.Seeta Rama Raju, J.Y. Park, H.C. Jung, H.K. Yang, B.K. Moon, J.H. Jeong, J.H. Kim, Synthesis and luminescent properties of low concentration $Dy^{3+}$:GAP nanophosphors, Optical Materials 31 (8) (2009) 1210–1214.

[10] X.Q. Wang, X.M. Han, C.M. Zhen, Study on energy transfer and energy migration of $Ca_2Gd_8(SiO_4)_6O_2:Dy^{3+}$ phosphor films, Journal of Nanoscience and Nanotechnology 11 (11) (2011) 9714–9716.

[11] G.Seeta Rama Raju, H.C. Jung, J.Y. Park, B.K. Moon, R. Balakrishnaiah, J.H. Jeong, J.H. Kim, The influence of sintering temperature on the photoluminescence properties of oxyapatite $Eu^{3+}:Ca_2Gd_8Si_6O_{26}$ nanophosphors, Sensors and Actuators B: Chemical 146 (1) (2010) 395–402.

[12] R. El Ouenzerfi, C. Goutaudier, G. Panczer, B. Moine, M.T. Cohen-Adad, M. Trabelsi-Ayedi, N. Kbir-Ariguib, Investigation of the $CaO–La_2O_3–SiO_2–P_2O_5$ quaternary diagram. Synthesis, existence domain, and characterization of apatitic phosphosilicates, Solid State Ionics 156 (1–2) (2003) 209–222.

[13] G.Seeta Rama Raju, J.Y. Park, H.C. Jung, B.K. Moon, J.H. Jeong, J.H. Kim, Luminescence properties of $Dy^{3+}:GdAlO_3$ nanopowder phosphors, Current Applied Physics 9 (Suppl. 2) (2009) e92–e95.

[14] J. Wan, L. Cheng, J. Sun, H. Zhong, X. Li, W. Lu, Y. Tian, H. Lin, B. Chen, Energy transfer and colorimetric properties of $Eu^{3+}/Dy^{3+}$ co-doped $Gd_2(MoO_4)_3$ phosphors, Journal of Alloys and Compounds 496 (1–2) (2010) 331–334.

[15] S. Das, A. Amarnath Reddy, G. Vijaya Prakash, Near white light emission from $K^+$ ion compensated $CaSO_4:Dy^{3+}$, $Eu^{3+}$ phosphors, Ceramics International 38 (7) (2012) 5769–5773.

[16] V.R. Bandi, B.K. Grandhe, H.-J. Woo, K. Jang, D.-S. Shin, S.-S. Yi, J.-H. Jeong, Luminescence and energy transfer of $Eu^{3+}$ or/and $Dy^{3+}$ co-doped in $Sr_3AlO_4F$ phosphors with NUV excitation for WLEDs, Journal of Alloys and Compounds 538 (0) (2012) 85–90.

[17] B. Wang, L. Sun, H. Ju, Luminescence and energy transfer of white-light emitting: phosphors, Solid State Communication 150 (31–32) (2010) 1460–1462.